journal

J. Am. Ceram. Soc., 80 [7] 1727–40 (1997)

Effect of Ordering-Induced Domain Boundaries on Low-Loss $Ba(Zn_{1/3}Ta_{2/3})O_3$–$BaZrO_3$ Perovskite Microwave Dielectrics

Peter K. Davies* and Jianzhu Tong

Department of Materials Science and Engineering, University of Pennsylvania, Philadelphia, Pennsylvania 19104–6272

Taki Negas*,†

Trans-Tech Inc., Adamstown, Maryland 21710

Small substitutions of $BaZrO_3$ into $Ba[(Zn,Ni)_{1/3}Ta_{2/3}]O_3$ are utilized in the commercial preparation of low-loss perovskite microwave dielectrics. The structures of a series of these phases with substitution levels ranging from 1% to 5% $BaZrO_3$ were examined using high-resolution TEM. For ≤ 2.15% $BaZrO_3$ the solid solutions retain the ordered ''1:2'' structure of the $Ba[(Zn,Ni)_{1/3}Ta_{2/3}]O_3$ end-member but are comprised of small ordered domains whose size decreases as the Zr content is raised. The decrease in the size of the domains parallels a decrease in the processing time required to access a low-loss state. Although for pure $Ba[(Zn,Ni)_{1/3}Ta_{2/3}]O_3$ reductions in the degree of cation order produce a large increase in the dielectric loss, the Zr-substituted ceramics retain a very low loss. We believe the low losses of the 1:2 ceramics are derived from the stabilization of the ordering-induced domain boundaries via the partial segregation of the Zr cations. For substitutions between 3% and 5% $BaZrO_3$ the size of the ordered domains continues to decrease but the system undergoes an abrupt transformation to a cubic ''1:1'' ordered structure with a doubled perovskite repeat. The structures of these phases have been interpreted using a ''random layer'' model in which one site is occupied by Ta and the other by a random distribution of Zn, Zr, and the remaining Ta cations, i.e., $Ba\{[Zn_{(2-y)/3}Ta_{(1-2y)/3}Zr_y]_{1/2}[Ta_{1/2}]\}O_3$. Although the ordering is confined to nano-sized domains, these ceramics also exhibit low losses, again reflecting the relative stability of the domain boundaries. In this case we believe the low losses reflect the effectiveness of the random layer in stabilizing the anti-phase boundaries.

I. Introduction

With the current worldwide explosion in the development of microwave-based communications technologies, the production of dielectric resonators has emerged as one of the most rapid growth areas in electronic ceramic manufacturing. Beginning in the 1970s several oxides were developed to satisfy the electronic and economic requirements for a commercial microwave resonator system. By combining a high relative permittivity ($\epsilon_r > 25$), a low dielectric loss or high Q ($Q = 1/\tan\delta > 5000$) and a near-zero temperature coefficient of resonant frequency ($\tau_f = 0 \pm 10$ ppm), microwave resonator ceramics in the BaO–TiO_2 ($Ba_2Ti_9O_{20}$, $BaTi_4O_9$), ZrO_2–SnO_2–TiO_2 ($Zr_{1-x}Sn_xTiO_4$), BaO–ZnO–Ta_2O_5 ($Ba(Zn_{1/3}Ta_{2/3})O_3$), and BaO–PbO–RE_2O_3–TiO_2 (e.g., $Ba_{6-3x}RE_{8+2x}Ti_{18}O_{54}$, RE = rare earth) systems have found widespread commercial application as filters and oscillators in wireless communication technologies.[1,2] While these ceramics are adequate for current applications, the drive toward further miniaturization and improved filtering capabilities will require the development of new oxides with higher dielectric constants and lower losses. Although some guidelines do exist, an understanding of the critical chemical and structural requirements for a successful ceramic resonator is only in its infancy. This progress has been impeded by the complex crystal chemistry of many of the existing oxide dielectric resonators, whose structures are often highly disordered through the formation of a wide variety of extended defects.[3–11] In this paper we present the results of a study in which high-resolution transmission electron microscopy (HRTEM) was used to correlate the local structure and dielectric loss properties of $Ba(Zn_{1/3}Ta_{2/3})O_3$ ceramics that contain low levels (≤5%) of $BaZrO_3$. It will be shown that the formation of ordering-induced domain structures plays an important role in determining the dielectric response.

In the 1980s a series of perovskite ceramics with Q factors exceeding 10 000 at 10 GHz were developed for high-frequency applications.[3,4] The perovskites found to exhibit the highest Q values are based on the formula $Ba(M^{2+}_{1/3}Ta^{5+}_{2/3})O_3$, where M = Zn, Mg. For the Zn system, $\epsilon_r \approx 30$, and for Mg, $\epsilon_r \approx 25$. Through the studies of Galasso and others several years ago, it is well known that most Ba- and Sr-based perovskites that contain a 1:2 mixture of divalent and pentavalent ions on the octahedral sites adopt a structure in which the two cations order onto individual (111) crystallographic planes.[12–14] The long-range ordering and associated correlated displacements of the oxygen anions between the cation planes yields a trigonal structure with a $\{..M^{2+}–M^{5+}–M^{5+}..\}$ repeat sequence along the ⟨111⟩ direction of the parent cubic perovskite cell which is coincident with the c direction of the supercell (see Fig. 1). Studies of the structures and electronic properties of the tantalate systems revealed that the degree of ordering of the M^{2+} and Ta^{5+} ions has a pronounced effect on the dielectric loss at microwave frequencies. By inducing long-range cation order through extended high-temperature (≥1400°C) annealing, the Q values of $Ba(Zn_{1/3}Ta_{2/3})O_3$ and $Ba(Mg_{1/3}Ta_{2/3})O_3$ ceramics can be increased from ~500 to >35 000 at 10 GHz.[3,4] Although other investigators suggested that the improvements in Q could be related to the volatilization of Zn,[15] several subsequent studies of magnesium and zinc tantalates, in which the volatilization was minimized or eliminated, have clearly demonstrated that the changes in the losses arise from alterations in the intrinsic degree of cation order.[4]

In previous studies of the relationship between the structure and dielectric loss properties of $Ba(Zn_{1/3}Ta_{2/3})O_3$ and $Ba(Mg_{1/3}Ta_{2/3})O_3$, powder X-ray diffraction methods were utilized to

P. P. Phule—contributing editor

Manuscript No. 191611. Received August 12, 1996; approved January 16, 1997.
Supported by the National Science Foundation under Grant No. DMR 94-21184 and through the National Science Foundation, MRSEC program, under Grant No. DMR 96-32598. The electron microscopy facility is supported by the National Science Foundation, MRSEC program, Grant No. DMR 96-32598.

*Member, American Ceramic Society.
†Current address: Dimag, Inc., Frederick, Maryland, 21703.

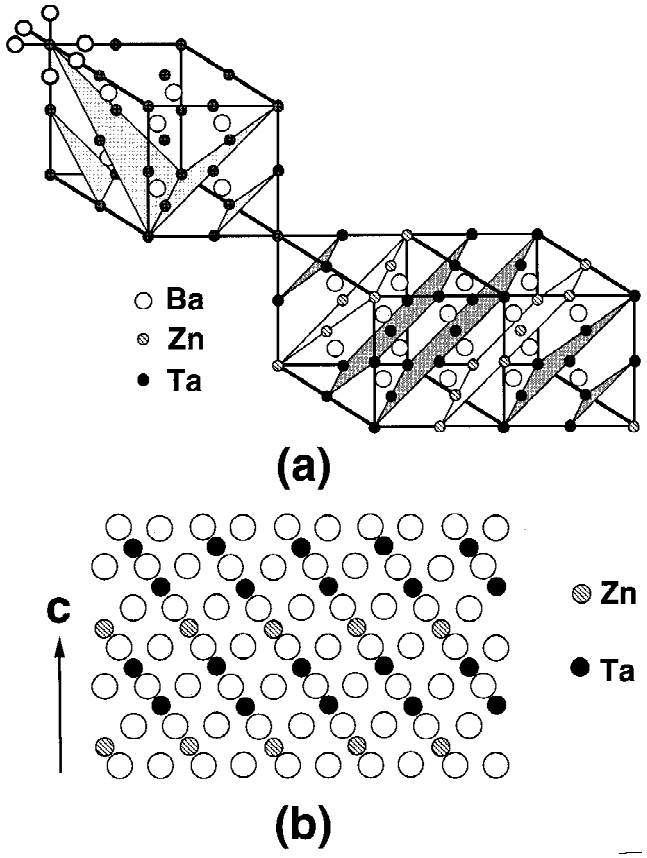

Fig. 1. Schematic illustration of 1:2 cation ordering in $Ba(Zn_{1/3}Ta_{2/3})O_3$: (a) Upper left shows two of the possible ⟨111⟩ directions for the ordering of Zn and Ta in the perovskite structure; lower right shows 1:2 ordering for one of the orientational variants. Oxygen anions omitted for clarity. (b) Idealized $[110]_{subcell}$ projection of the ordered structure; large open circles, oxygen anions; large shaded circles, Ba cations; the anions that project onto the A-site positions are omitted for clarity.

investigate the variation of the ordering of the B-site cations with the firing conditions (annealing temperature and time).[3,4,16] The principal signatures of the cation-ordering used to evaluate the relationship of the structure to Q were the appearance and relative changes in intensity of the superlattice peaks originating from the chemical order, and the splitting of reflections associated with the deviation of the c/a ratio of the ordered trigonal structure from the value expected for an ideal undistorted unit cell (where $c/a = (3/2)^{1/2} = 1.2247$). The ''degree of order'' has been gauged through an order parameter (S) where $S = \sqrt{[(I_{100}/I_{110,012})_{obs}/(I_{100}/I_{110,012})_{calc}]}$; $(I_{100}/I_{110,012})_{obs}$ is the ratio of the observed intensity of the (100) superstructure reflection to that of the (110) and (012) reflections from the subcell, and $(I_{100}/I_{110,012})_{calc}$ is the corresponding ratio calculated for a fully ordered structure using published structural data.[14] The lattice distortion arises from a small expansion of the parent cubic cell in a direction normal to the ordered (111) planes and a ''fully ordered'' hexagonal structure has $c/a > 1.2247$. The most significant improvements in Q with annealing occur when $S > 0.75$; these also coincide with the appearance and increase in the lattice distortion associated with the long-range chemical order.[16]

While the fully ordered barium–tantalum-based perovskites have outstanding losses and can be tuned to a zero τ_f, for example by partial substitution of the Zn ions in $Ba(Zn_{1/3}Ta_{2/3})O_3$ ($\tau_f = 3$ ppm/°C) by Ni ($Ba(Ni_{1/3}Ta_{2/3})O_3$, $\tau_f = -17$ ppm/°C), the long annealing times required to access a high-Q state prevented commercialization of these ceramics. In 1984 Tamura *et al.* showed this barrier could be overcome through minor additions of $BaZrO_3$, typically less than 5 mol%, which dramatically reduce the annealing times, to ≤10 h, required to reach the high-Q state.[17] Therefore, commercial high-Q perovskite dielectrics are formulated from a mixture containing ≈ 89% $Ba(Zn_{1/3}Ta_{2/3})O_3$, 7.5% $Ba(Ni_{1/3}Ta_{2/3})O_3$, and 3.5% $BaZrO_3$, and have $\epsilon_r \approx 29$, $Q > 12000$ at 10 GHz with $\tau_f = 0$.

Although the studies of the pure $Ba(Ma^{2+}_{1/3}Ta_{2/3})O_3$ (M = Zn, Mg, Ni) perovskites appear to have yielded a consistent picture of the relationship between cation order, the associated structural distortions, and the dielectric loss, the behavior of the $BaZrO_3$-doped systems is not as straightforward. In their study of the large reduction in the annealing time required to reach high Q, Tamura *et al.* examined the microwave properties and cell geometry of $Ba(Zn_{1/3}Ta_{2/3})O_3$–$BaZrO_3$ and $Ba(Zn_{1/3}Ta_{2/3})O_3$–$SrTiO_3$ solid solutions.[17] For the substitution of $BaZrO_3$ the Q values at 7 GHz increased from 10 000 to 15 000 for additions up to approximately 4 mol%, gradually decreased to 10 000 for $X_{BaZrO_3} = 0.25$, and then degraded more rapidly for higher concentrations (see Fig. 2). In the $SrTiO_3$-doped system Q deteriorated rapidly for all concentrations. It was also noted that both substitutions accelerated the ''crystallization'' of the perovskite structure and the low-$BaZrO_3$-doped samples yielded high-Q ceramics after very short annealing times (4 h at 1500°C). Perhaps the most surprising result, particularly in light of the well-documented improvement of Q with increased cation order in the Zr-free tantalate, was the observation that the X-ray lines associated with the long-range ordering had disappeared in the 4% $BaZrO_3$ high-Q samples. The low concentration additions of $SrTiO_3$ had a similar effect on the structural order, though in this case the Q's were inferior to the undoped sample.[17]

The report on the reduction in the annealing time required to produce a high Q in the $Ba(Zn_{1/3}Ta_{2/3})O_3$–$BaZrO_3$ system has been reproduced by several groups and these additions are currently used to produce commercial resonators. However, the origins of the improved Q's, the decrease in the time required to reach high Q, and the observation of an apparently disordered distribution of B-site cations at very small levels of $BaZrO_3$ substitution remain unexplained. Furthermore, the formation of a high-Q ceramic with a random cation distribution seems to contradict the experimental and theoretical studies of the undoped tantalate systems. Despite their importance, no detailed structural studies of the Zr-substituted perovskites have been made.

Before we present the results of our TEM investigations of the $Ba(Zn_{1/3}Ta_{2/3})O_3$–$BaZrO_3$ system, it is useful to reconsider the cation ordering reactions in $Ba(M^{2+}_{1/3}Ta_{2/3})O_3$ ''1:2'' perovskites. When these phases are first prepared, they crystallize in an apparently ''disordered'' cubic perovskite structure. With extended annealing the ''degree of order,'' as gauged by the intensity and sharpness of the superlattice lines in the X-ray patterns, increases and as a ''completely ordered'' structure is approached the unit cell undergoes a small hexagonal

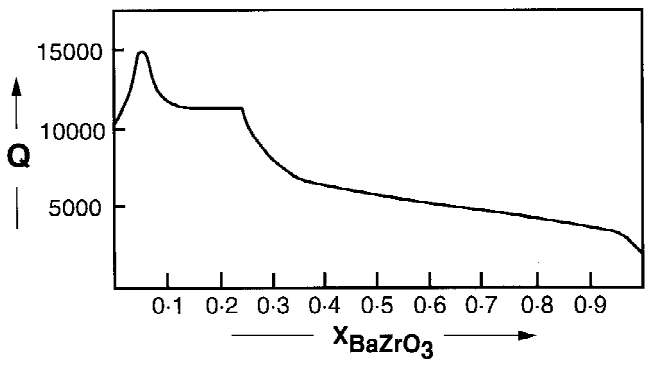

Fig. 2. Variation of Q with composition in the $Ba(Zn_{1/3}Ta_{2/3})O_3$–$BaZrO_3$ system; data are redrawn from Ref. 17.

distortion. While the use of an order parameter S might imply this transformation is second order and reversible, under the conditions used during their synthesis and processing the ordering reactions in these systems are irreversible and controlled by kinetic rather than thermodynamic factors. As noted in the first studies made by Galasso,[12,13] a more correct description of the evolution of these phases is in terms of the nucleation and growth of small ordered domains with increasing annealing time and temperature. Because of the significant line broadening associated with small domain sizes, accurate measurements of the true structural state of these systems, i.e., the degree of order within the domains and the domain size, using X-ray or neutron methods requires careful analysis of the peak widths and intensities using profile refinement methods. Although most previous studies of $Ba(M^{2+}_{1/3}Ta_{2/3})O_3$ (M = Zn and Mg) have not used this type of analysis, recent structure refinements of the closely related $Sr(Al^{3+}_{1/2}M^{5+}_{1/2})O_3$ (M^{5+} = Nb, Ta) systems have confirmed the validity of the domain nucleation/growth mechanism.[18]

The formation of an ordering-induced domain structure necessarily implies that ''partially ordered'' samples contain high levels of unstable domain boundaries. For the trigonal 1:2 structure two different types of boundaries are possible. The first is a twin boundary separating different orientational variants in which the nucleation and growth of the ordered structure have propagated along different [111] orientations of the cubic subcell; four discrete variants are possible (see Fig. 1). The second is an anti-phase boundary (APB) associated with each set of ordering orientations. From an energetic and structural viewpoint, the boundaries are highly unfavorable as they produce a region with local cation disorder and considerable associated elastic strain. While the previous interpretations of the decrease in Q with reduced ''cation order'' have focused on the degree of chemical ordering between M^{2+} and Ta^{5+}, the importance of losses associated with the formation of the domain boundaries has been overlooked.

The primary objectives of our TEM studies of the $(1-x)Ba[(Zn,Ni)_{1/3}Ta_{2/3}]O_3$–$xBaZrO_3$ system were to understand (1) the sensitivity of Q to the ordering of the Zn and Ta cations for $X_{BaZrO_3} \leqslant 0.05$, (2) if and how the substitution of $BaZrO_3$ inhibits the cation ordering, and (3) why the introduction of low levels of $BaZrO_3$ reduce the time required to process these systems to a high-Q state.

II. Experimental Procedure

Ceramics in the $(1-x)Ba[(Zn,Ni)_{1/3}Ta_{2/3}]O_3$–$xBaZrO_3$ system with the compositions shown in Table I were prepared from commercially available powders of $BaCO_3$, Ta_2O_5, ZnO, ZrO_2, and NiO. In all cases the powder purities were >99.8%. As the Zr content of the samples was increased, the ratio of Zn:Ni was systematically raised to maintain a near-zero temperature coefficient of resonant frequency. Because the crystal chemistry of Ni and Zn is so similar in this system, we believe the small alterations in the relative concentrations of the two divalent ions does not have any significant effect on the results described below. Stoichiometric concentrations of the powders were blended by high shear mixing and the slip (70% solids) was gelled with acetic acid. The blend was calcined at 1000°C to remove CO_2 and avoid initial Zn loss. The calcine was rehomogenized in a vibratory mill under distilled water for 1 h and then recalcined at 1300°C. This calcine ensures that Zn is stabilized in the perovskites, reduces its vapor pressure, and obviates the need to cover the parts after pressing and firing. All the symptoms of Zn loss, which are usually a result of using poorly blended or pre-reacted powder, such as lack of densification or a low-density white skin around the fired parts, were avoided by using the double precalcine procedure. After the precalcines the powders were vibratory milled to an average of 1 μm under distilled water, spray dried using PVA, and isostatically pressed at 10 000 psi. The final sintering was conducted at 1510°C. All samples were fired until they reached a high Q value (>10 000 at 10 GHz). For the ceramics containing 1.25% Zr this required at least 24 h, for 2.15% Zr 16 h, and for 3%, 4.25%, and 5% Zr 8 h. In each case additional annealing did not produce any significant improvement in Q.

The relative permitivity of the samples was measured in the GHz range using the parallel plate method combined with a network analyzer and computer.[19,20] The accuracy of the measurement by this technique is better than ±0.25%. Measurements of the dielectric loss, $Q = 1/\tan\delta$, and the temperature coefficient of resonant frequency, τ_f, at microwave frequencies were made using cavity methods.[21] The τ_f values refer to the 25–60° range according to $\tau_f = \Delta f \cdot f_o \Delta T$, where f_o is the reference frequency at 25°C. The Q values reported in Table I were all measured at 10 GHz. The reproducibility of the Q and τ_f measurements is better than ±5% and ±0.7ppm/°C, respectively. For all ceramics the relative permittivity was between 28 and 31 and τ_f was 0±4 ppm.

Samples for transmission electron microscopy were prepared by disaggregating the ceramic followed by grinding under acetone in an agate mortar. The powder was then suspended in acetone and dispersed onto a holey carbon 200 mesh TEM grid. Transmission electron microscopy was performed with 300 kV (Model 430T, Philips Electronic Instruments, Mahwah, NJ) and 400 kV microscopes (Model 4000EX, JEOL, Boston, MA).

Powder X-ray diffraction was conducted using a Rigaku DMAX-B diffractometer with a conventional Cu$K\alpha$ source. Lattice parameters were calculated by least-squares refinement of powder diffraction data collected using silicon powder as an internal standard.

III. Results

The X-ray patterns of selected samples listed in Table I are shown in Fig. 3. For 1.25% $BaZrO_3$ the pattern 3(a) contains reflections from the hexagonal superstructure and can be indexed using a cell with $a = 0.5775(1)$ nm, $c = 0.7100(2)$ nm, $V = 0.2051(1)$ nm^3, and $c/a = 1.229$. An order parameter $S = 0.99$ was calculated from the integrated intensities of the background subtracted X-ray pattern using the approach described previously. In the pattern of samples with 2.15% $BaZrO_3$ (Fig. 3(b)) the superlattice peaks were considerably broader (FWHM = 0.33° 2θ as compared to 0.28° 2θ for 1.25% $BaZrO_3$); the larger peak width made reliable calculation of the integrated intensities more difficult but yielded $S \approx 0.75$. This sample could still be indexed to a hexagonal cell with $a = 0.5788(1)$ nm, $c = 0.7089(1)$ nm, $V = 0.2056(1)$ nm^3, and $c/a = 1.225$. From the line broadening the size of the ordered domains was estimated to be ≈35–40 nm. For $BaZrO_3$ concen-

Table I. Composition and Dielectric Properties of $(1-x)Ba(Zn/Ni_{1/3}Ta_{2/3})O_3$–$xBaZrO_3$ Samples

[$BaZrO_3$] (mol%)	Composition	Q (10 GHz)	ε_r	τ_f (ppm/°C)
1.25	$Ba_3(Zr_{0.0375}Zn_{0.790}Ni_{0.1975}Ta_{1.975})O_9$	11 448	28.2	−5
2.15	$Ba_3(Zr_{0.0645}Zn_{0.816}Ni_{0.1625}Ta_{1.957})O_9$	12 686	28.7	−2
3.0	$Ba_3(Zr_{0.090}Zn_{0.845}Ni_{0.125}Ta_{1.940})O_9$	10 018	29.3	1
4.25	$Ba_3(Zr_{0.1275}Zn_{0.885}Ni_{0.0725}Ta_{1.915})O_9$	11 909	29.7	2
5.0	$Ba_3(Zr_{0.150}Zn_{0.9125}Ni_{0.0375}Ta_{1.900})O_9$	10 634	30.7	4

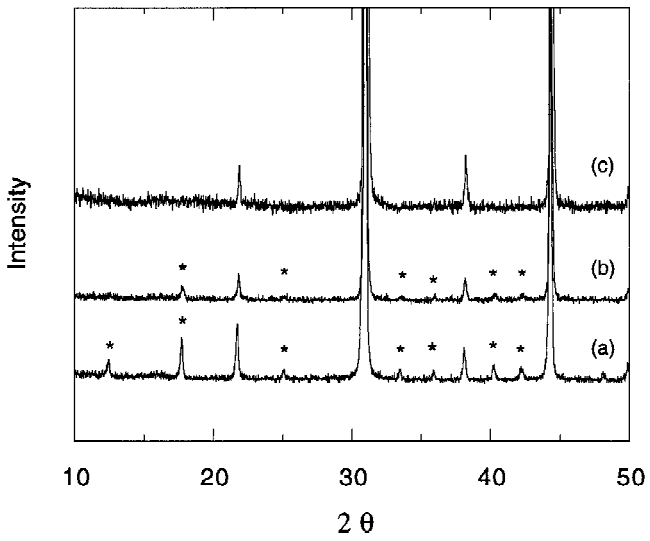

Fig. 3. X-ray powder diffraction patterns of $Ba(Zn_{1/3}Ta_{2/3})O_3$ solid solutions with (a) 1.25%, (b) 2.15%, and (c) 3.0% $BaZrO_3$. Superlattice reflections from 1:2 order are highlighted.

trations between 3% and 5% the X-ray powder patterns showed no evidence for cation order and could all be indexed with an ideal cubic perovskite cell; the pattern from a sample with 3% $BaZrO_3$ is shown in Fig. 3(c). Cell parameter refinements gave a = 0.40950(5) nm, 0.40976(2) nm, and 0.40983(4) nm for 3%, 4.25%, and 5% $BaZrO_3$, respectively.

An electron diffraction pattern collected from 1.25% $BaZrO_3$ along the [110] direction of the pseudocubic perovskite subcell is shown in Fig. 4(a). The strong superlattice reflections visible at positions of ($h \pm 1/3$, $k \pm 1/3$, $l \pm 1/3$) from the fundamental reflections originate from the chemical order and correspond to the tripling of the cell along one unique ⟨111⟩ direction. Lattice images of this sample (Fig. 5) indicated that the structure was close to perfectly ordered. Occasional twin and anti-phase boundaries were observed in some grains. From analyses of the lattice images of several grains the size of the ordered domains, i.e., the average separation of anti-phase or twin boundaries, was found to be >200 nm.

The images and diffraction patterns collected from samples containing 2.15% $BaZrO_3$ revealed a quite different situation. In this case the superlattice reflections at ($h \pm 1/3$, $k + 1/3$, $l + 1/3$) in the [110] selected area diffraction patterns were observed along both of the allowed ⟨111⟩ directions (Fig. 4b)), implying that the diffracting volume is comprised of a twinned, ordered domain structure. Lattice images (see Fig. 6) collected from the same area of the sample confirm this interpretation and provide direct evidence for the formation of ordered domains with a twin relationship. In this image contrast modulations with a periodicity corresponding to $\frac{1}{3}$⟨111⟩ (~0.71 nm) are evident in different regions of the grain along each of the two allowed ⟨111⟩ directions. The higher-resolution image in Fig. 7 was collected using an objective aperture which allowed contributions from the (001), (110), $\frac{1}{3}$(111), and $\frac{2}{3}$(111) reflections. In this image several different areas of image contrast can be discerned. The contrast in areas A and B originates from the ordering of the cations along each of the two in-plane ⟨111⟩ directions of the parent perovskite cell; this type of contrast accounts for approximately 50% of the area of the image. In the areas labeled C the modulations associated with the ordering are absent and the only contrast visible is that associated with the parent perovskite subcell. A fourth type of contrast is visible in the regions (D) of overlap of the ordered domains.

Computer simulations of the image contrast expected from the 1:2 ordered structure of $Ba(Zn(Ni)_{1/3}Ta_{2/3})O_3$ were made using the atom positions reported in Ref. 14 assuming complete ordering of Zn and Ta and a {..ZnTaTa..} repeat along ⟨111⟩. The calculated images were in excellent agreement with the contrast observed in regions A and B of the high-resolution images. From an analysis of the symmetry of the 1:2 structure (space group P-3m1, point group 4/m-32/m of order 48) and the parent perovskite subcell (space group Pm-3m, point group −32/m of order 12) it is apparent that four equivalent ⟨111⟩ orientational variants of the cation-ordered structure are possible. For any given $[110]_{subcell}$ zone axis contrast differences associated with the ordering of the B cations are only visible for the two trigonal variants that have their c axes oriented perpendicular to the beam direction. The two out-of-zone variants will only exhibit contrast normally associated with a disordered structure. We believe the regions labeled C in Fig. 7, which constitute approximately 50% of the area of the image, correspond to the two out-of-zone ordered variants of the $Ba(Zn_{1/3}Ta_{2/3})O_3$ structure.

The size and shape of the ordered domains in the 2.15% $BaZrO_3$ sample are somewhat irregular, as are the boundaries separating the various orientational variants. On average the correlation length of the cation order within the ordered (111) planes of the domains is approximately 40 nm and twice that along the perpendicular direction, i.e., the c direction of the hexagonal cell. In several regions of the grains it is apparent that different orientational variants overlap within the depth of the crystal. It is this overlap that produces the additional coincidence fringe contrast visible in the regions labeled D in Fig. 7.

As the concentration of $BaZrO_3$ is raised to 3–5%, the size of the ordered domains continues to diminish; however, the higher levels of substitution also induce an abrupt change in the periodicity of the cation ordering. In addition to very weak and diffuse spots at ($h \pm 1/3$, $k + 1/3$, $l + 1/3$), the [110] diffraction patterns of 3%$BaZrO_3$ (Fig. 4(c)) contain superlattice reflections at ($h \pm 1/2$, $k \pm 1/2$, $l \pm 1/2$). The appearance of these new reflections is consistent with the formation of a face-centered cubic supercell with a periodicity twice that of the primitive perovskite subcell. Additional reflections at ($h + 1$, $k + 1/2$, $l + 1/2$) were also present in the diffraction patterns of samples with 4.25% (Fig. 4(d)) and 5% (not shown) $BaZrO_3$; for these compositions there is no residual intensity at ($h \pm 1/3$, $k \pm 1/3$, $l \pm 1/3$).

The occurrence of the so-called ''F spots'' at ($h \pm 1/2$, $k \pm 1/2$, $l \pm 1/2$) has been reported in a number of mixed-metal perovskites. This type of superstructure is commonly observed in $A(B'_{1/2}B''_{1/2})O_3$ systems where the formation of the face-centered cubic supercell results from the chemical ordering of B′ and B″ in alternate (111) planes (see Fig. 8).[22–24] Similar diffraction patterns have also been reported in the $Pb(Mg_{1/3}Nb_{2/3})O_3$ (PMN) and $Ba(Zn_{1/3}Nb_{2/3})O_3$ ''1:2'' systems,[23,24] though the nature of the chemical order that gives rise to the doubling of the periodicity is still a matter of some debate. While in these examples it is the positional ordering of the B′ and B″ ions that gives rise to the superlattice reflections, identical diffraction effects can arise from correlated tilting of the oxygen octahedra in the perovskite structure.[26,27] To discriminate between these two possibilities, chemical order and octahedral tilting, the samples with diffraction maxima at $\frac{1}{2}$⟨111⟩ were examined between −165° and 800°C using controlled temperature stages. [110] patterns that were collected at −165°, 700°C and room temperature from the 3% $BaZrO_3$ sample are shown in Fig. 9. For this and the 4.25% and 5% samples, the relative intensity of the $\frac{1}{2}$⟨111⟩ reflections was independent of temperature. These results support the conclusion that the doubling of the perovskite cell between 3% and 5% $BaZrO_3$ is the result of chemical ordering on the B sites rather than octahedral tilting which is typically very sensitive to temperature.

Lattice images of the 3% $BaZrO_3$ sample that were collected using contributions from the (001), (110), and $\frac{1}{2}$(111) reflections are shown in Figs. 10 and 11. In addition to the lattice fringes from the parent perovskite subcell, both images contain contrast modulations along the {111} direction with a period-

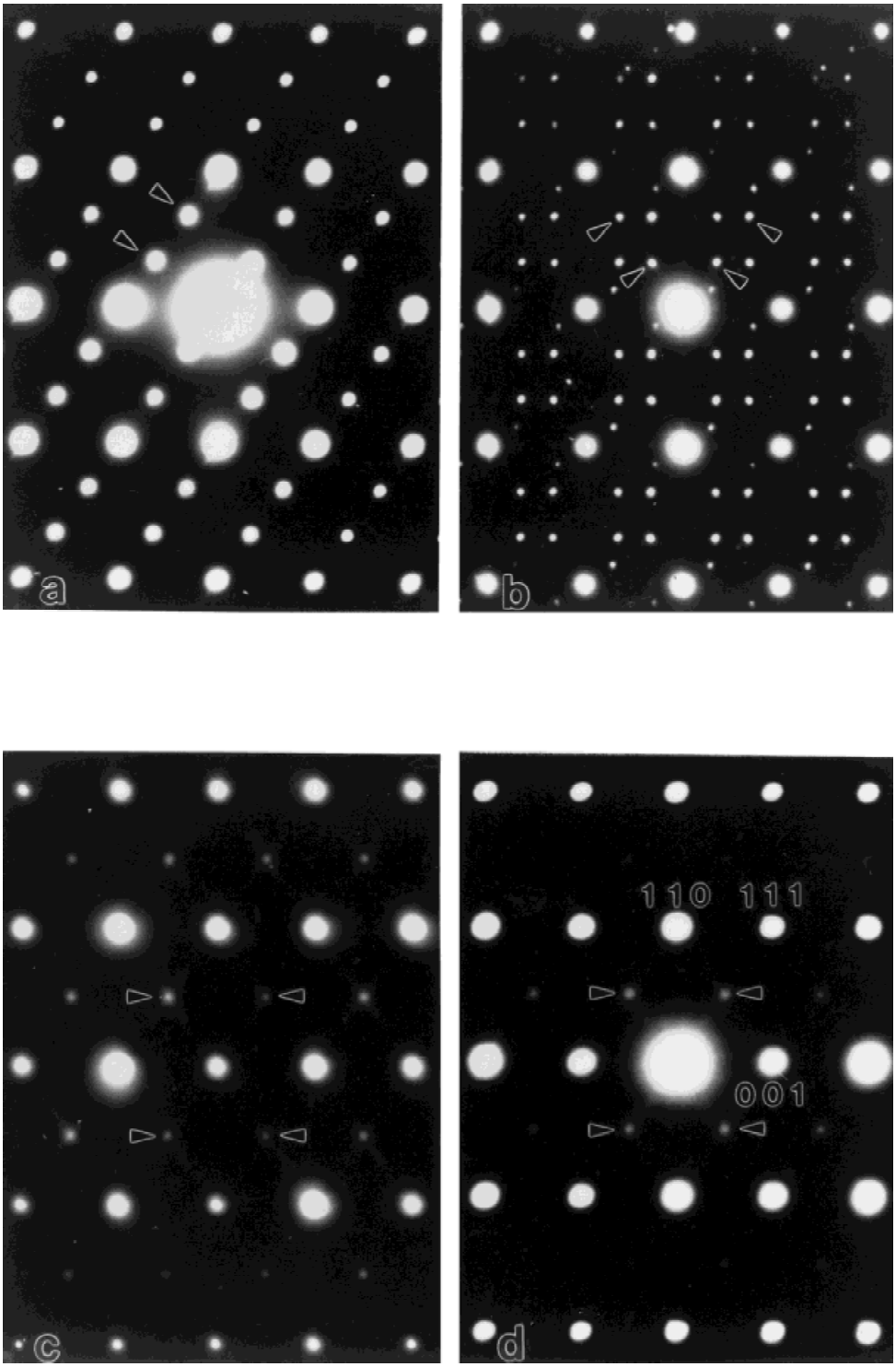

FIG. 4. Electron diffraction patterns collected along [110] of the perovskite subcell for (a) 1.2%, (b) 2.15%, (c) 3.0%, and (d) 4.25% $BaZrO_3$.

icity, ~0.47 nm, that corresponds to the $\frac{1}{2}\{111\}$ superlattice reflections observed in the electron diffraction patterns. As expected considering the weak and diffuse nature of the $\frac{1}{2}\{111\}$ reflections, the cation correlations in these samples are short and the additional contrast in the images indicates that the structure is comprised of ordered domains approximately 2–4.5 nm in size. While the lower-magnification image in Fig. 10 provides evidence for the uniform distribution of the ordered regions throughout the sample, the contrast from the $\frac{1}{2}\{111\}$ modulations shows many disruptions and distortions associated with the short correlation length of the cation order. The contrast from the supercell formation was also unusually sensitive to changes in defocus as well as sample thickness.

The contrast associated with the cation ordering is more apparent in the higher-magnification image in Fig. 11, where it is possible to identify a pseudohexagonal array of white spots within the ordered domains. In some regions of this image the ordering modulations are very weak and difficult to discern, particularly in the regions separating the ordered domains. On viewing the images in Figs. 10 and 11 along either of the (111) directions it is apparent that the contrast modulations in different domains are frequently displaced by $\frac{1}{2}(111)_{\text{ordered}}$ and that

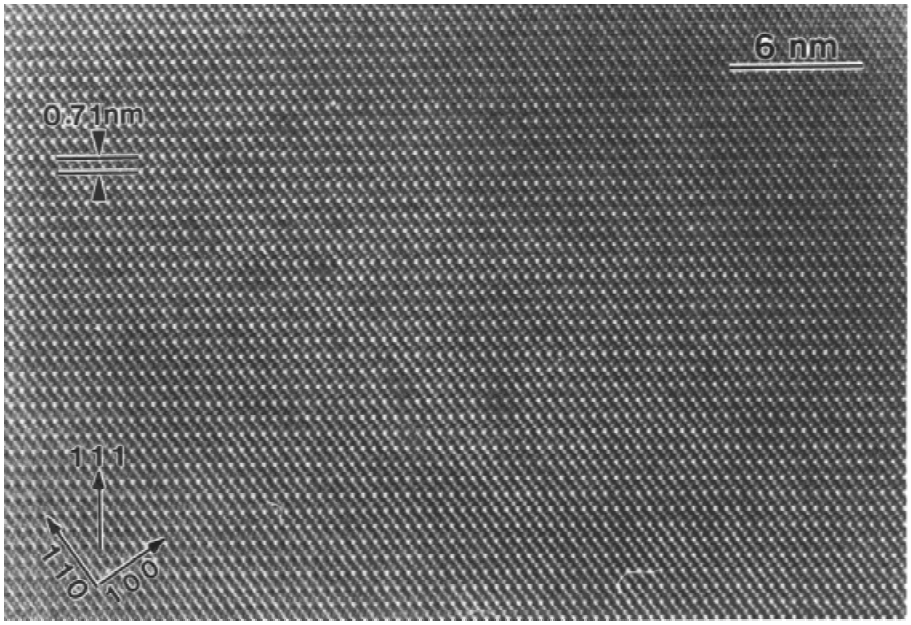

Fig. 5. Lattice image collected along $[110]_{subcell}$ from solid solutions with 1.25% $BaZrO_3$.

many of the domains show an anti-phase relationship. It is these displacements that seem to be responsible for the apparent wavy nature of some of the 0.47 nm fringes in Fig. 10. The importance of the APBs in the interpretation of the structure and properties of these systems will be discussed later.

The high-resolution images collected from samples with 4.25% and 5% $BaZrO_3$ were very similar to those observed for the 3% substituted ceramics. Figure 12 shows a region of the 5% $BaZrO_3$ sample in which the size, 2–4.5 nm, contrast, and anti-phase relationship between the domains are apparent.

IV. Discussion

Powder diffraction patterns collected using a conventional X-ray source indicate that the introduction of 3–5% $BaZrO_3$ into $Ba(Zn_{1/3}Ta_{2/3})O_3$ eliminates the ordering of the metal cations on the octahedral sites of the perovskite lattice. However, our analyses using electron optical techniques clearly show that these compositions are in fact ordered and that the substitution of $BaZrO_3$ induces a series of complex changes in the cationic correlations over a very narrow range of chemical composition. In this section we will address the changes in the length scale and nature of the cation order that accompany the substitution of $BaZrO_3$, examine how these can be consistent with the high Q values of the ceramics, and correlate the formation of the ordered domain structures to the large reductions in the annealing times required to access a low-loss state.

A summary of the TEM results for the compositions in the $Ba(Zn_{1/3}Ta_{2/3})O_3$–$BaZrO_3$ system examined in this study is shown in Table II. For $\leq$2.15% $BaZrO_3$ the solid solutions retain a trigonal structure with a 1:2 ordering of alternate layers of Zn(Ni) and Ta along the ⟨111⟩ directions of the parent perovskite cell. Although these very low levels of substitution do not change the geometry of the cation ordering, they do

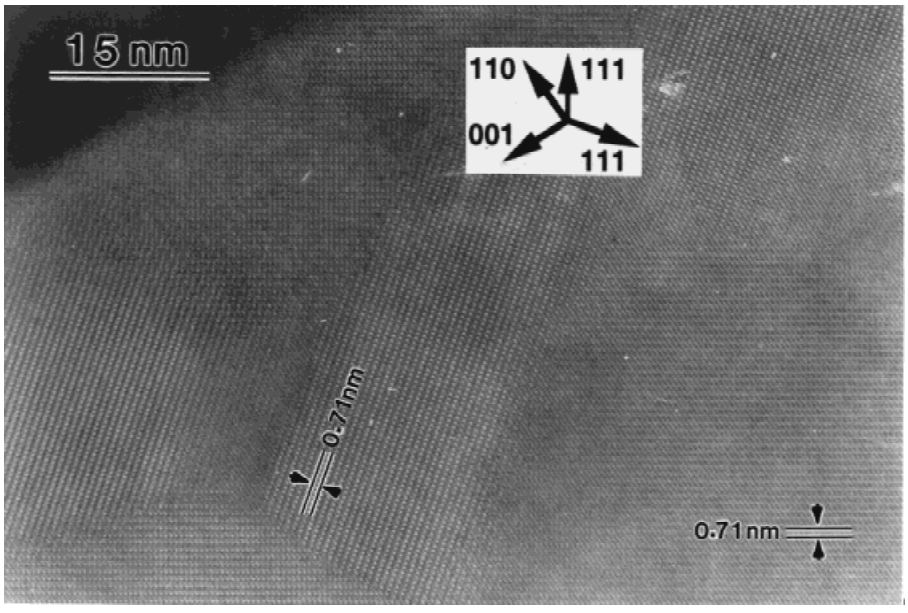

Fig. 6. [110] lattice image from samples containing 2.15% $BaZrO_3$. Fringes from the two in-zone, 1:2 ordered variants are highlighted.

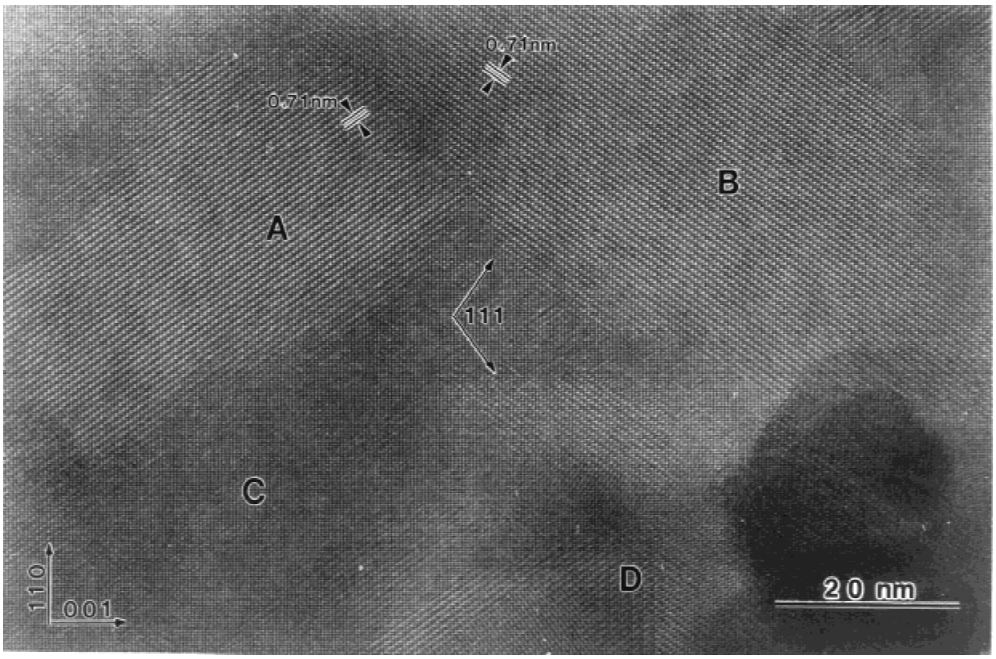

Fig. 7. [110] image from 2.15% $BaZrO_3$. Four different types of fringe contrast correspond to the two in-zone ordered variants (A and B), the out-of-zone 1:2 variants (C), and domain overlap in the beam direction (D).

reduce the length-scale of the cation correlations. From the contrast in the lattice images the average size of the ordered domains decreases from >200 nm for 1% $BaZrO_3$ to ~40 nm for 2.15% substitution. An indication of these microstructural changes is also provided by the differences in the height and width of the superlattice reflections in the corresponding powder X-ray diffraction patterns.

As the concentration of $BaZrO_3$ is increased to 3–5%, the high-resolution images and electron diffraction patterns provide evidence for a continued reduction in the cationic correlations and the formation of a structure comprised of 2.5–4 nm domains. These higher level substitutions also modify the geometry of the cation ordering and stabilize a face-centered cubic supercell with a doubled repeat. The change from trigonal to cubic symmetry occurs over a very narrow range of composition, between 2.15% and 3% $BaZrO_3$. The lack of any significant change in the intensity of the $\frac{1}{2}\langle 111\rangle$ reflections with temperature was considered sufficient evidence to rule out the possibility that the doubling of the perovskite cell arises from a correlated octahedral tilting transformation. It was concluded that these supercell reflections arise from chemical ordering of the cations on the octahedral sites. Because the range of the ordering is so limited, the only reflections detectable by a standard X-ray probe for these compositions are those originating from the parent cubic perovskite subcell.

One of the goals of this work was to understand why the substitution of $BaZrO_3$ into $Ba(Zn_{1/3}Ta_{2/3})O_3$ decreases the processing time required to access a high-Q state. It seems likely that this effect is directly related to the large reduction in the size of the chemically ordered domains induced by the addition of $BaZrO_3$. While the decrease in domain size might explain the accelerated kinetics, the large increase in the volume of domain boundaries that accompanies the substitution implies that Zr is also effective in reducing the losses associated with the boundary regions. In the absence of any substituent the Q value of ''partially ordered'' $Ba(Zn_{1/3}Ta_{2/3})O_3$ is very low, a result, we believe, of the very high losses at the elastically strained domain boundary regions. While extended thermal treatments can be used to reduce the volume of the boundaries and improve the loss properties of pure $Ba(Zn_{1/3}Ta_{2/3})O_3$, apparently the same result can be achieved by lowering the losses of the boundary regions through incorporation of an

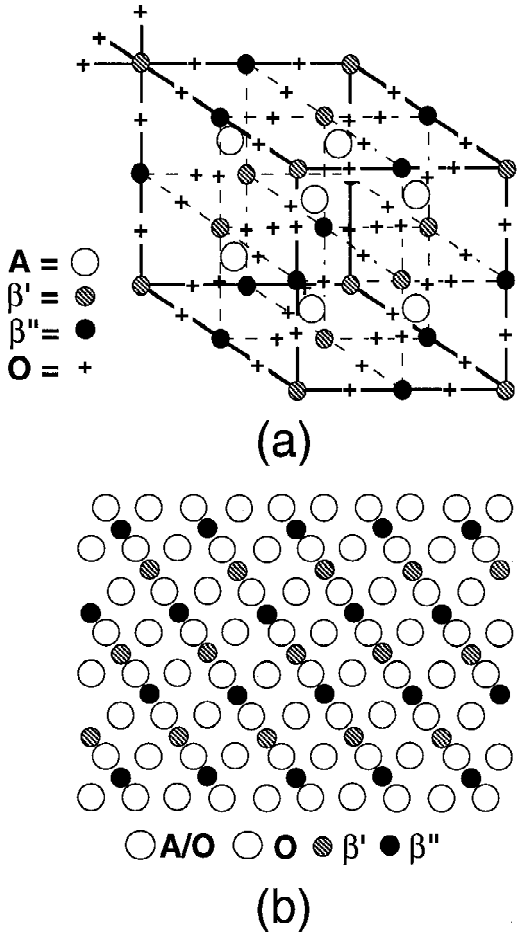

Fig. 8. (a) Schematic representation of the doubled cubic perovskite cell of the 1:1 $A(\beta'_{0.5}\beta''_{0.5})O_3$ ordered structure (b) idealized $[110]_{subcell}$ projection; anions projecting onto the A-site positions are omitted.

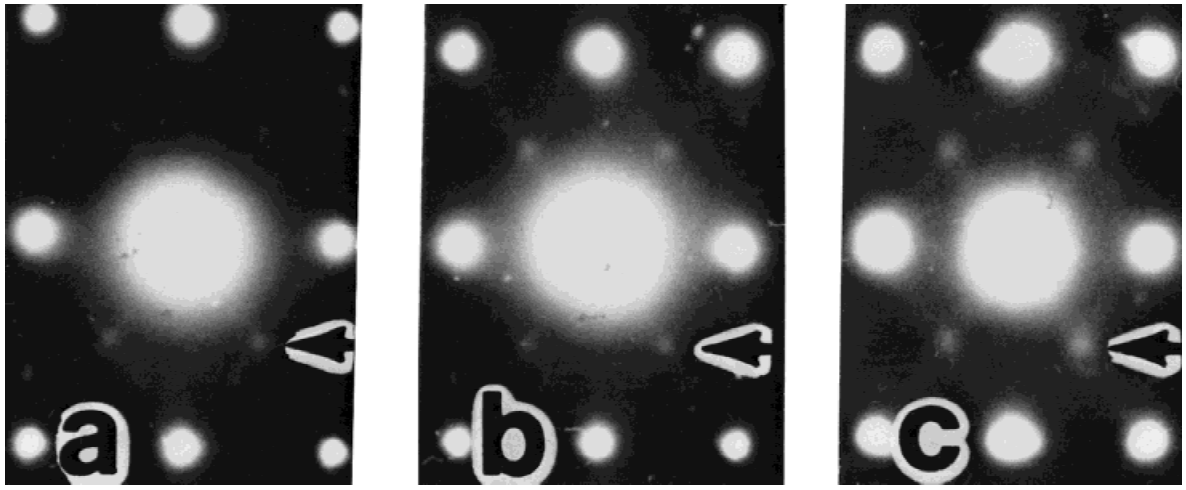

Fig. 9. [110] diffraction patterns collected from 3% $BaZrO_3$ at (a) −165°C, (b) room temperature, (c) 700°C. Arrows point to $\frac{1}{2}\langle 111\rangle$ reflections.

''appropriate'' chemical dopant. For the region of stability of the 1:2 ordered structure we propose that the stabilization of the domain boundary is achieved via the preferential segregation of the Zr cations. This conclusion, which will be discussed below, is supported by the observed increase in the boundary volume with increasing Zr content and is also consistent with previous studies that we have made on the role of Sn dopants in stabilizing ordering-induced boundaries in low-loss $ZrTiO_4$ microwave resonators.[6]

(1) 0–2.15% $BaZrO_3$: Low-Loss, 1:2 Ordered Domain Structures

The transformation of cubic perovskite to a trigonal 1:2 ordered structure can produce four equivalent orientational variants in which the *c* axis of the ordered cell is oriented along one of the $\langle 111\rangle$ directions of the parent subcell. Each orientational form, with a cell volume 3 times that of the subcell, has three different translational variants which bear an anti-phase relationship. During the growth of the ordered structure the impingement of different domains can produce twin and anti-phase boundaries that separate the different orientational and translational variants. The occurrence of the domain boundaries raises the free energy of the system by introducing local changes in the chemical stoichiometry, by increasing coulombic repulsions through alterations in the nearest-neighbor cation coordination, and by disrupting the long-range displacements of the anions that accompany the cation ordering. The magnitude of the destabilization necessarily depends upon the orientation of the boundary. For example, twin boundaries parallel to either the (100) or (110) directions of the perovskite subcell (see Fig. 13(a)) are conservative and also induce the smallest perturbation to the nearest-neighbor cation coordination. Depending on their location, boundaries parallel to $(111)_{subcell}$, i.e., parallel to the basal plane of one of the ordered domains (Fig. 13(b)), produce a localized enrichment of either Zn or Ta and also introduce the largest number of ''wrong'' nearest-neighbor cations. Perhaps the major destabilizing feature of the boundaries is their effect upon the concerted displacements of the oxygen anion layers that accommodate the different bond lengths of the two B-site cations. These displacements must be reversed on crossing the boundary to the adjacent domain. When the boundary has a component parallel

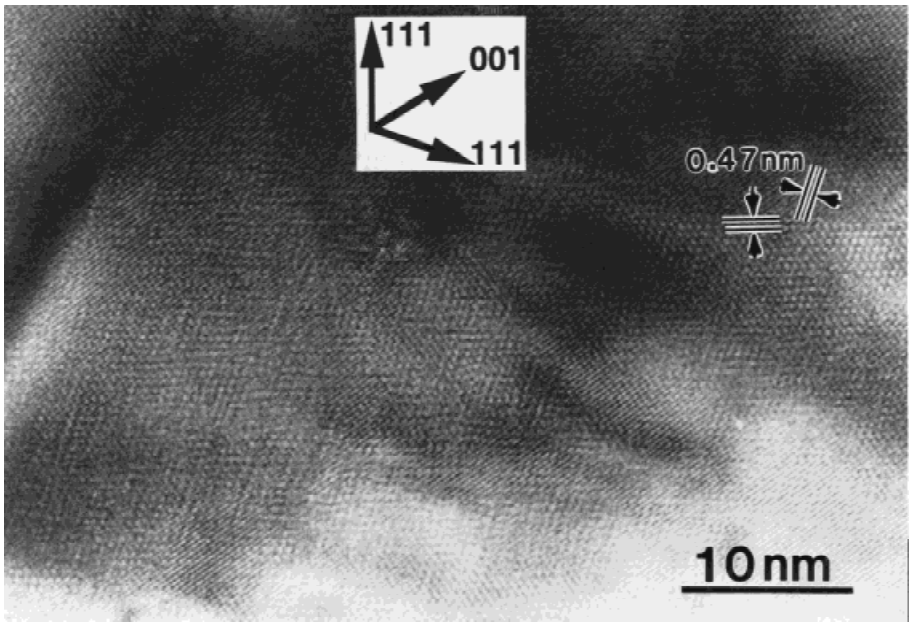

Fig. 10. Lattice image showing nano-domain 1:1 structure in 3% $BaZrO_3$.

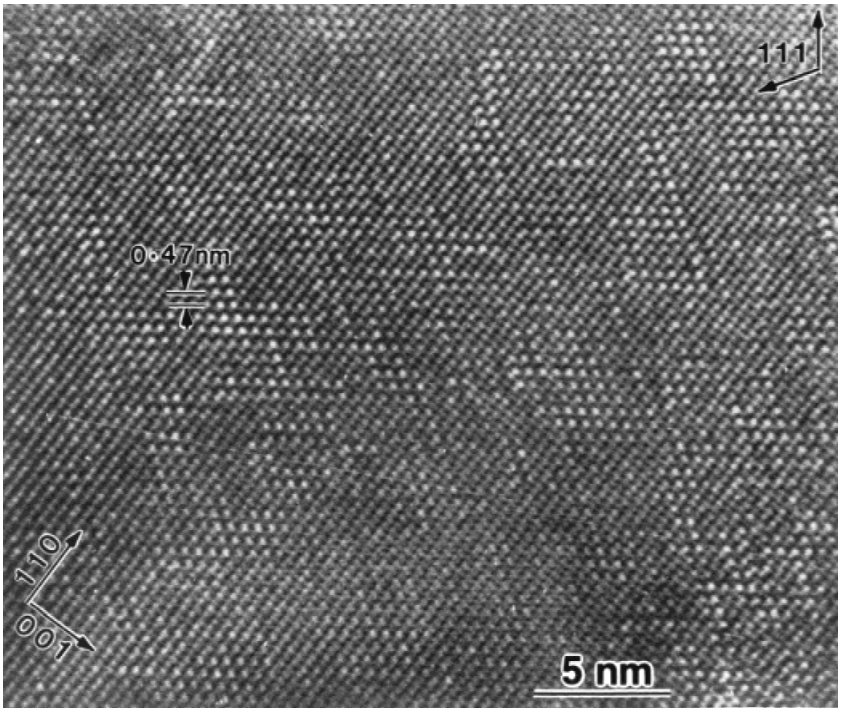

Fig. 11. Higher-resolution image of 1:1 domain structure in 3% $BaZrO_3$.

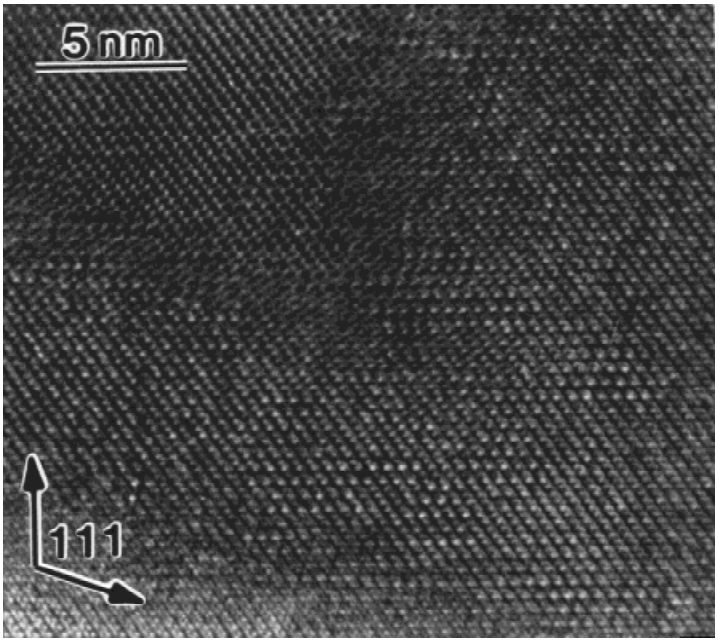

Fig. 12. Lattice image collected from samples containing 5% $BaZrO_3$.

to the *c* axis of the ordered structure, it will intersect and disrupt all of the anion layers in the surrounding domains. In contrast, when the boundary is parallel to the basal plane of an ordered domain, i.e., parallel to $(111)_{subcell}$, it only intersects the layer of anions adjacent to the interface.

The [110] lattice images collected from 2.15% $BaZrO_3$ provide the best information on the preferred orientations and differing energetics of the boundaries in the 1:2 structure. These images (Figs. 6 and 7) contain modulations from the two in-zone orientational variants and their associated translational forms. The domains are highly anisotropic, the correlation along the *c* axis of the ordered structure is approximately half that along the basal plane direction, and most adjacent domains have a twin rather than anti-phase relationship. The ''flattening'' of the domains implies that the energies of the boundaries

Table II. Summary of HRTEM Results for $(1 - x)Ba(Zn/Ni_{1/3}Ta_{2/3})O_3$–$xBaZrO_3$

$BaZrO_3$ (%)	Domain size (nm)	Ordering	Anneal time (h)	*Q* (10 GHz)
1.25	⩾200	1:2	24	11 448
2.15	20–40	1:2	16	12 686
3.0	2.5–5	1:1 + (trace 1:2)	8	10 018
4.25	2.5–5	1:1	8	11 909
5.0	2.5–5	1:1	8	10 634

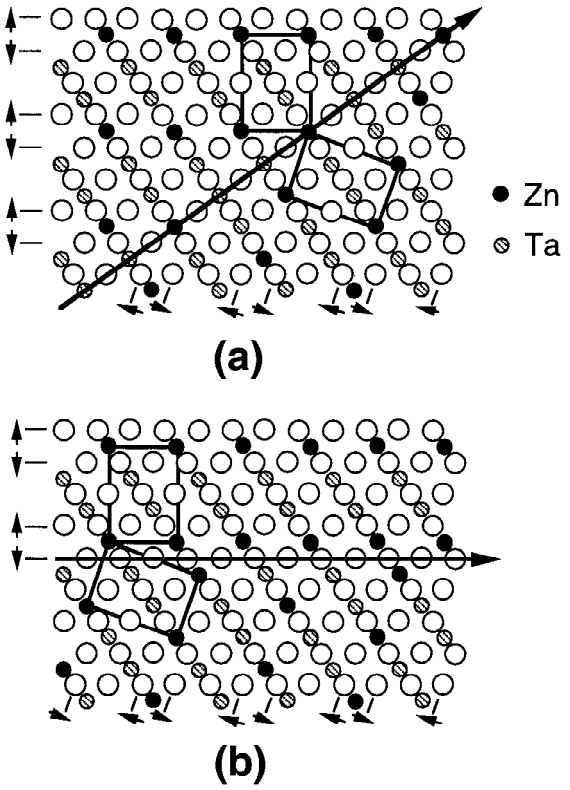

Fig. 13. Idealized representation of domain boundary formation in the 1:2 ordered structure of $Ba(Zn_{1/3}Ta_{2/3})O_3$: (a) boundary parallel to (110), (b) parallel to (111). Large open circles represent oxygen anions; arrows indicate direction of concerted anion displacements toward smaller Ta cation sites.

along *c* are higher than those parallel to the basal plane of the ordered structure. This conclusion is supported by the orientations of the majority of the boundaries visible in the images which, although they have considerable fine structure, typically lie parallel to the basal plane of one of the adjacent ordered variants. The apparent preference for the termination of the domains on $(111)_{subcell}$ implies that the minimization of the anion layer disruptions is the primary factor affecting the morphology and stability of the 1:2 domain structures.

In the absence of added dopants that could segregate and mediate the destabilizations, it is not surprising that the elastic strains, unfavorable coulombic interactions, and chemical inhomogeneities associated with the domain boundaries in $Ba(Zn_{1/3}Ta_{2/3}O)_3$ are a source of dielectric loss. The excess energies associated with the disruption of the cation order and anion displacements at the boundaries can be expected to be in the same range as the free energy for cation disordering, which in this system is very high. Our observation that the Zr-substituted ceramics can sustain a low loss, even though they contain a high concentration of domain boundaries, suggests that the boundary regions are somehow stabilized, perhaps through the preferential segregation of the Zr^{4+} ions. Although thermodynamic considerations require that some Zr ions are necessarily introduced into the Zn and Ta layers in the ordered domains, the transformation to a different ordering scheme at 3% $BaZrO_3$ shows the substitution has a very unfavorable effect on the energetics of the 1:2 structure. The loss of 1:2 order at such low levels of Zr implies that the destabilization is not simply a short-range effect, but that longer-range interactions, such as the concerted oxygen anion displacements, are frustrated by the large mismatch in the Ta–O and Zr–O bond lengths. While the preferential partitioning of Zr to the boundaries during the growth of the ordered domains would alleviate, to some degree, the unfavorable energetics associated with the bulk substitution, it could also lower the energies of the domain boundaries that would otherwise result (see Fig. 14). The valence of Zr is equal to the mean valence of the octahedral lattice sites in the unsubstituted perovskite; therefore, its segregation could reduce the coulombic destabilizations of the Zn^{2+} and Ta^{5+} ions at the boundary regions without violating the overall charge balance of the structure. The lattice parameter of $BaZrO_3$ is slightly larger than the $Ba(Zn_{1/3}Ta_{2/3})O_3$ subcell which may also be beneficial providing a stable interfacial ''buffer layer'' at the otherwise elastically strained domain boundaries. The partial segregation of Zr to the boundaries is consistent with the observed decrease in the domain size and the associated increase in the volume of boundaries with higher levels of $BaZrO_3$.

Because the charge and size of Zr^{4+} appear to be critical in its ability to stabilize the boundary regions, Sn^{4+} could also be an effective substituent while the smaller size of Ti^{4+} may inhibit its use as a boundary segregant. Additional support for the importance of the substituent size comes from the high *Q* values that have been reported for $BaSnO_3$-substituted $Ba(Mg_{1/3}Ta_{2/3})O_3$ ceramics,[29] whereas additions of $SrTiO_3$ to $Ba(Zn_{1/3}Ta_{2/3})O_3$ were shown to have an adverse effect on *Q*.[17]

(2) 3–5% $BaZrO_3$: Low-Loss, 1:1 Ordered Nano-domains

When the concentration of $BaZrO_3$ is raised to 3%, the symmetry of the ordering is modified and the system adopts a face-centered cubic ($Fm3m$) structure with $a = 2a_{per}$. This phase boundary coincides with the anomaly in *Q* reported previously for this system by Tamura *et al.*[17] (see Fig. 2). The electron diffraction patterns and lattice fringe contrast of the samples with 3–5% $BaZrO_3$ are very similar to those observed in ''1:1''-type $A(B'_{0.5}B''_{0.5})O_3$ perovskites, where the doubled cell edge results from an ordering of the B′ and B″ cations in alternate β′ and β″ layers of the $A(\beta'_{0.5}\beta''_{0.5})O_3$ structure.[22–24] The enthalpic stability of this superstructure, which is also known as the $(NH_4)_3FeF_6$ structure (see Fig. 8) is again derived from the minimization of coulombic cationic repulsions, each B′ atom has six B″ nearest neighbors, and from the displacement of the oxygen anions to accommodate the B′–O and B″–O bond length mismatch. Chemically ordered 1:1 structures have also been observed in some ''1:2'' mixed-metal perovskites. For example, the lead-based $Pb(M^{2+}_{1/3}M^{5+}_{2/3})O_3$ relaxor ferroelectrics (M^{2+} = Mg, Ni, Zn, etc.; M^{5+} = Nb, Ta)[23–25] and the hexavalent $A(M^{6+}_{1/3}M^{3+}_{2/3})O_3$ systems (A = Ba, Sr; M^{3+} = Al, Fe, Sc, rare earth; M^{6+} = W, U, Re)[22,29–32] all adopt a ''1:1''-type ordered arrangement.

Two different models have been proposed for the chemistry of the ordered β′ and β″ cation layers in the 1:1 structures of 1:2 perovskites. In the $Pb(M^{2+}_{1/3}M^{5+}_{2/3})O_3$ systems, where the ordering is restricted to nano-sized domains, it has been suggested that the β′ and β″ layers are occupied exclusively by the M^{2+} and M^{5+} ions, respectively.[23,25,33] To conserve overall

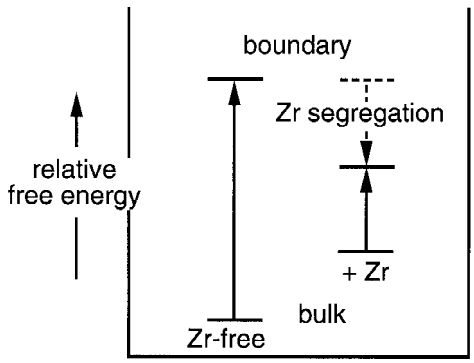

Fig. 14. Schematic representation of the relative energies of the bulk (bottom) and boundary (top) regions in the Zr-free (left), and Zr-substituted (right) 1:2 ordered form of $Ba(Zn_{1/3}Ta_{2/3})O_3$.

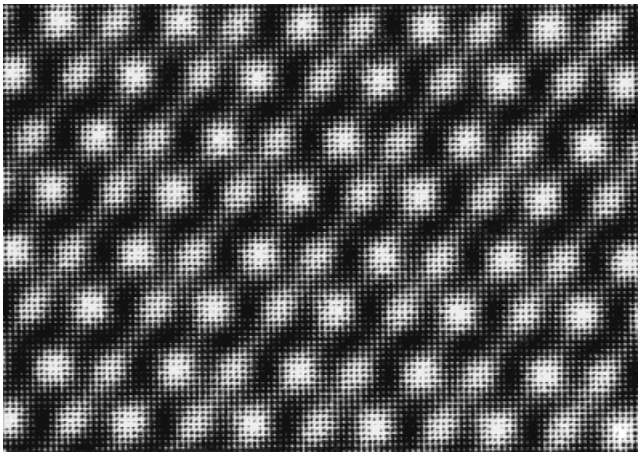

Fig. 15. Simulation of the (110) lattice images of 1:1 ordered 3% $BaZrO_3$ samples using the random layer model (see text); image shown corresponds to a thickness of 3.5 nm, and a defocus of −55 nm.

electroneutrality the charge imbalance within the 1:1 ordered region is assumed to be compensated by an equal and oppositely charged, M^{5+}-rich disordered matrix that surrounds the nano-domains. Support for this two-phase ''space charge'' model has come primarily from the apparent lack of coarsening of the ordered domains upon annealing; however, it should be noted that no definitive, direct evidence for this type of atomic level compositional segregation has as yet appeared in the literature. Although it has not found widespread acceptance, other researchers have proposed that the 1:1 order in the 1:2 perovskites could be explained using a ''random layer'' model.[34–36] In this ordering scheme the β′ layer contains a random distribution of M^{2+} and M^{5+} in a 2:1 ratio while the β″ layer is occupied exclusively by M^{5+} cations. In the random layer model, where the perovskite can be represented as $A\{[M^{2+}_{2/3}M^{5+}_{1/3}]_{1/2}[M^{5+}]_{1/2}\}O_3$, the 1:1 domains are charge balanced and a 1:2 ratio of the M^{2+} and M^{5+} ions is maintained in all regions of the sample.

In the $(1 - x)Ba(Zn_{1/3}Ta_{2/3})O_3$–$xBaZrO_3$ system the transformation from 1:2 to 1:1 order is induced by the introduction of very small levels of Zr^{4+}. Because the 1:1 phase is stabilized by the incorporation of Zr^{4+}, it is hard to rationalize the ordering in terms of a space-charge model with a 1:1 distribution of Zn and Ta in the domains. If this was the case, a 1:1 structure would also be expected for the $Ba(Zn_{1/3}Ta_{2/3})O_3$ end-member. Instead we favor a ''random layer'' model in which the β″ sites in the 1:1 domains are occupied by Ta^{5+} and the Zr cations enter the β′ sites which contain a random distribution of Zn^{2+}, Zr^{4+}, and the remaining Ta^{5+} ions. In this model the formula of the ordered 1:1 form of the $(1 - x)Ba(Zn_{1/3}Ta_{2/3})O_3$–$xBaZrO_3$ solid solutions can be rewritten as $Ba\{[Zn_{(2-y)/3}Ta_{(1-2y)/3}Zr_y]_{1/2}[Ta_{1/2}]\}O_3$, where $y = 2x$. Although the fitting was impeded by the limited range of the cation correlations within the ordered domains (which affect the quality of the experimental high-resolution data), for thicknesses comparable to the domain size (~3.5 nm) the image simulations of the 3–5% substituted solid solutions using the random layer model (y = 0.06–0.1) were in good agreement with the contrast observed in the high-resolution images (see Fig. 15).

Because the concentration of Zn:Ta in the random layer of a 1:1 $Ba(Zn_{1/3}Ta_{2/3})O_3$ end-member would be 2:1, but their replacement by Zr is in a 1:2 ratio ($yZr^{4+} = (y/3)Zn^{2+} + (2y/3)Ta^{5+}$), it is apparent that the random layer model for the 1:1 solid solutions could be valid for compositions up to 25% $BaZrO_3$, i.e., $y \leq 0.5$. It is at this composition that a second anomaly in the Q values of this system was reported by Tamura *et al.*[17] (Fig. 2). Additional investigations to explore the phase stabilities at higher $BaZrO_3$ compositions have confirmed this interpretation and will be the subject of a separate publication (Chai and Davies, in preparation).

The formation of a 1:1 random layer structure is consistent with the crystal chemical reasoning used above to interpret the domain structures and loss properties of the 1:2 ordered phases. The large reduction in the cation correlation lengths in the region of stability of the 1:2 structure (≤2.15% $BaZrO_3$) shows that the enthalpic stability of the ⟨111⟩ ordered layers of Zn and Ta is highly disrupted by the introduction of the Zr^{4+} ions. At such low levels of substitution we believe that localized interactions are unlikely to be solely responsible for the destabilization and that the longer-range anion displacements are frustrated by the addition of the Zr cations. The transformation to a 1:1 random layer structure for ≥3% $BaZrO_3$ appears to be an energetic compromise in which the long-range ordering of Ta in one layer is preserved at the expense of the others. While the enthalpic stability of the 1:1 random layer structure is clearly less favorable than that of the unsubstituted 1:2 ordered phase, but more so than a completely disordered perovskite or perhaps a partially substituted 1:2 structure, the entropic contributions to the overall free energies of these systems should not be overlooked. A random distribution of cations in every other ⟨111⟩ layer of the 1:1 structure introduces a significant favorable contribution to the free energy. The magnitude of the configurational entropy for the random $[Zn_{(2-y)/3}Ta_{(1-2y)/3}Zr_y]$ layer is shown as a function of y in Fig. 16, where for 1 mol of cations in the random layer

$$S_{\text{config}} = -R\{[(2 - y)/3] \ln [(2 - y)/3] + [(1 - 2y)/3] \ln [(1 - y)/3] + y \ln y\} \quad \text{J/(mol · K)}$$

From Fig. 16 it is apparent that very small concentrations of $BaZrO_3$ produce a large increase in S_{config}. For example, the entropy of the β′ random layer at 3% substitution (y = 0.06, S_{config} = 6.74 J/(mol · K)) is 27% larger than a Zr-free layer (y = 0.0, S_{config} = 5.29 J/(mol · K)). It is at this composition that the transformation from 1:2 to 1:1 order was observed in the electron diffraction experiments. The configurational entropy of the 1:1 structure at 3% substitution ($S_{\text{config/layer}}$ = (0 + 6.74)/2 = 3.37 J/(mol·K) is also significantly higher than the entropy expected for a random distribution of the Zr ions in the Zn and Ta layers of the 1:2 ordered structure, where $S_{\text{config/layer}}$ = 1.12 J/(mol·K). We suggest that the increase in entropy of the random layer structure and the decrease in the enthalpic stability of the 1:2 phase for small levels of substitution of $BaZrO_3$ are both responsible for the stabilization of the 1:1 ordered phases.

While the samples with 3–5% $BaZrO_3$ all adopt an ordered cubic 1:1 structure, the high-resolution micrographs presented in Figs. 10–12 show that the cation correlations are restricted to nano-sized domains. It is also evident from Fig. 11 that the contrast from the ordering is either absent or very weak in the

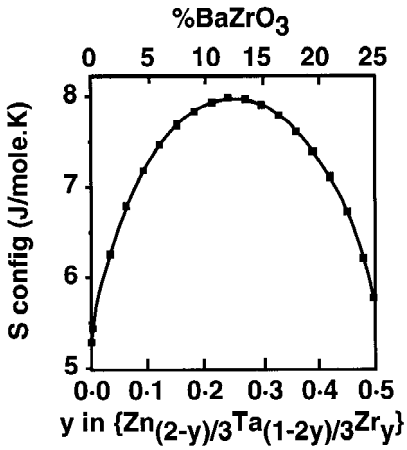

Fig. 16. Configurational entropy, S_{config}, of the $[Zn_{(2-y)/3}Ta_{(1-2y)/3}Zr_y]$ random layer as a function of the concentration of Zr (mol% $BaZrO_3$ and y).

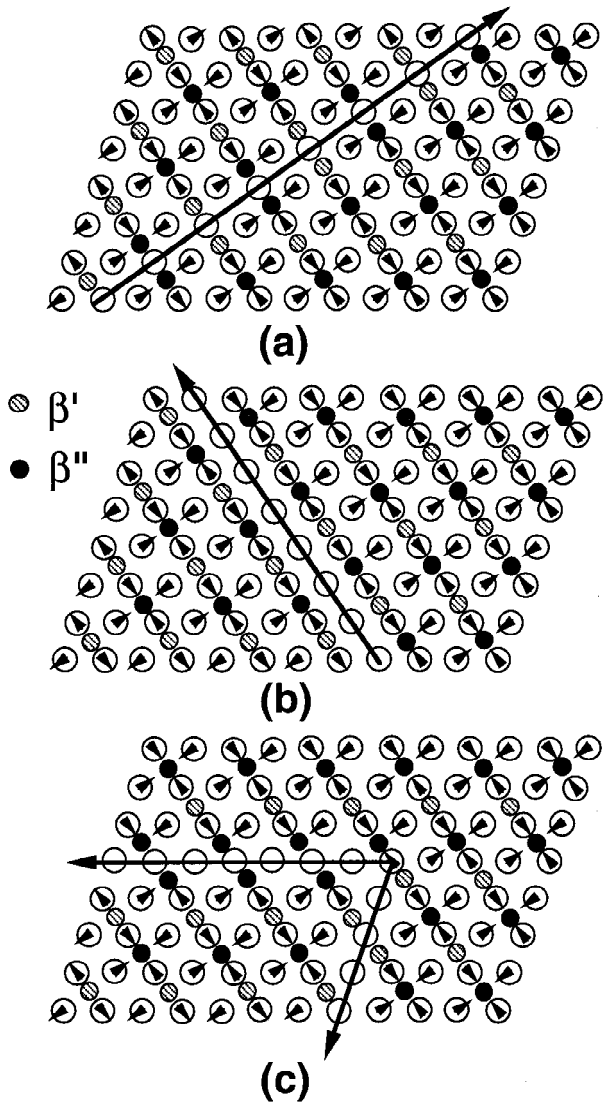

Fig. 17. Idealized view of anti-phase boundary formation in the 1:1 $A(\beta'_{0.5}\beta''_{0.5})O_3$ ordered structure for boundaries parallel to (a) (110), (b) (100), (c) (111). Large open circles represent oxygen anions; arrows indicate anion displacements toward smaller cation site.

regions separating the domains. For the 1:2 phases the lack of additional contrast in some regions of the [110] images can arise from the formation of different orientational variants of the ordered trigonal structure. Because the point group symmetry of the perovskite subcell and *Fm3m* supercell are identical, the 1:1 structure has only one orientational variant; therefore, all regions of the samples that are ordered should produce superlattice contrast along each of the [110] zone axes. However, the ordering correlations can still be perturbed by the formation of two different translational variants which are related by the displacement vector $R = a_{dis} = \frac{1}{2}a_{ord}$. The formation of translational variants is evident in the experimental images where the relative displacement of the ⟨111⟩ supercell fringes by $\frac{1}{2}\langle 111\rangle_{subcell}$ confirm the anti-phase relationship of the nano-scale 1:1 ordered domains. The absence of ⟨111⟩ supercell modulations in the areas between the domains may reflect the loss of cation order at the anti-phase boundaries though the variations in the intensity of the supercell modulations could also arise from overlap of the nano-sized ordered variants in the beam direction.

Even though the volume fraction of domain boundaries in the 1:1 ordered phases is very high, the losses of these ceramics in the 3–5% region are still very low. This would imply that the elastic strains at the boundary regions are again stabilized to the extent that they have no significant adverse effect on *Q*. Earlier it was argued that the segregation of Zr could be responsible for the lowering of the losses of the domain boundaries in the 1:2 ordered structures. In that case the driving force for the segregation is derived from both the high excess energies of a Zr-free boundary and the unfavorable energetics of the bulk substitution of Zr into the 1:2 structure. For the 1:1 phases this argument no longer holds as the incorporation of Zr into the random layer structure is responsible for its stabilization. It is our opinion that the low energies of the APBs, in the nano-domain 1:1 phases are directly attributable to the presence of the random layer in the structure. To clarify our reasoning for this conclusion it is useful to recall the behavior of other mixed-metal $A(\beta'_{1/2}\beta''_{1/2})O_3$ perovskites. In the $A(M^{3+}_{1/2}M^{5+}_{1/2})O_3$ phases, where the β′ and β″ sites are occupied exclusively by a single type of cation, kinetic factors can inhibit the formation of an APB-free structure; however, the ordered domains readily coarsen upon annealing, implying that the excess energies associated with the APBs are very high. This is easily understood in terms of the disruptions of the anion displacements, nearest-neighbor cation coordination numbers, and deviations from stoichiometry that could occur at the APB. In contrast the 1:1 ordered nano-domain structures of the 1:2 perovskites, which we believe are best understood in terms of the random layer model, show little coarsening with extended annealing (e.g., $Pb(Mg_{1/3}Nb_{2/3})O_3$) or exhibit very low dielectric losses (e.g., $Ba(Zn_{1/3}Ta_{2/3})O_3$–$BaZrO_3$). For these systems the stability of the 1:1 random layer structure is not as dependent upon an enthalpic contribution to the ordering free energy, but is more reliant upon the entropy associated with the random distribution of the M^{2+}, M^{5+} (and Zr^{4+} for $Ba(Zn_{1/3}Ta_{2/3})O_3$–$BaZrO_3$) cations on the β′ sites of the lattice. Therefore, the excess free energy of an APB in the 1:1 random layer structure of a 1:2 perovskite will be significantly lower than in the ''fully ordered'' 1:1 structures of the 1:1 perovskite systems (see Fig. 18).

Because localized alterations in the occupancy of the β′ sites in the random layer can occur without significant energetic penalty, we propose that a mechanism exists to further reduce the excess boundary energy in the 1:1 random-layer structures of the 1:2 perovskites. For example, an enrichment in the Ta occupancy of the β′ sites at an APB could delocalize and minimize the disruption of the anion displacements on crossing the boundary into the β″ (Ta) layer of an adjacent domain. By compensating this Ta enrichment through a corresponding depletion in the occupancy of Ta in the β′ positions at the

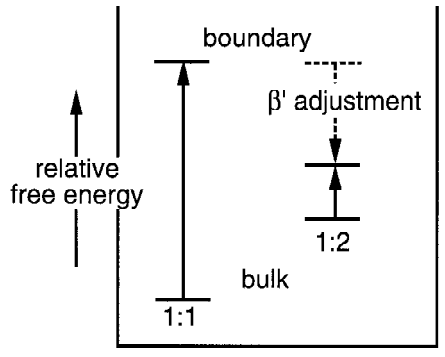

Fig. 18. Relative energies of the ordered bulk (bottom) and locally disordered domain boundaries (top) in the 1:1 $A(\beta'_{0.5}\beta''_{0.5})O_3$ structure. The left part of the diagram represents the excess boundary energy for a 1:1 perovskite where the β′ and β″ sites are occupied by a single type of cation (i.e., B′:B″ = 1:1); the right shows corresponding energies for the 1:1 ''random layer'' form of a 1:2 perovskite where B′:B″ = 1:2. Note the potential lowering of the boundary energy through a localized adjustment of the occupancy of the random layer sites (β′) at the boundary.

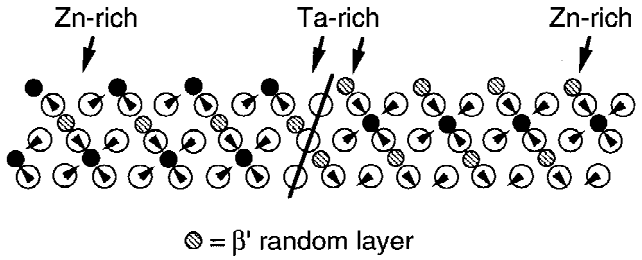

Fig. 19. Mechanism for stabilization of APBs in the 1:1 random layer form of a 1:2 perovskite. Localized enrichments of Ta in the random layer sites at the APB (arrowed) can partially delocalize and stabilize the reversal in the anion displacements at the boundary. The stoichiometry of the random layer is preserved through a corresponding enrichment of Zn in the near boundary regions (arrowed).

near-boundary regions, the localized segregation would be achieved without perturbing the overall stoichiometry of the random layer (see Fig. 19). This type of self-stabilization mechanism could significantly stabilize and delocalize the perturbations at the APB, reduce the driving force for domain coarsening, and minimize the dielectric loss (see Fig. 18). This model can only be effective in a 1:1 structure that contains a random layer; in the absence of an added dopant that could segregate to the boundary, no such mechanism exists for 1:1 systems where both the β' and β'' sites are fully occupied by a single type of cation.

V. Conclusions

The substitution of $BaZrO_3$ into low-loss $Ba(Zn_{1/3}Ta_{2/3})O_3$ microwave ceramics induces a series of complex changes in the ordering of the cations on the octahedral sites of the perovskite structure. At very low levels of substitution, $\leq$2.15%, the solid solutions retain the ordered 1:2 structure of the $Ba(Zn_{1/3}Ta_{2/3})O_3$ end-member, but are comprised of ordered domains whose size decreases as the Zr concentration is increased. The reduction in the cation correlations parallels the decrease in annealing time required to access a low-loss state. For pure $Ba(Zn_{1/3}Ta_{2/3})O_3$, reductions in the degree of cation order produce very large increases in the dielectric loss. The absence of any reduction in Q for Zr-substituted samples that contain a very high volume of domain boundaries suggests that Zr is effective in stabilizing the boundaries. We propose that this may be due to the preferential segregation of Zr to the boundary regions. As the level of substitution is increased to 3–5%, the size of the ordered domains continues to decrease but the symmetry of the cation ordering is changed and a cubic ''1:1'' structure with a doubled perovskite repeat is observed. The structure of the 1:1 phase was interpreted using a ''random layer'' model in which the ordering arises from an alternation of a Ta layer with a second layer that contains a random distribution of the Zn, Zr, and residual Ta cations. Ceramics in this compositional range also exhibit very low losses which we again interpret as reflecting, at least in part, the relative stability of the domain boundaries. We believe the low losses of the 1:1 nano-domain structures result from the effectiveness of the random layer in stabilizing the APBs. The transformations in the ordering of the B-site cations in the $Ba(Zn_{1/3}Ta_{2/3})O_3$–$BaZrO_3$ system occur at the same compositions that had been previously reported to show anomalous changes in the loss properties.[17]

Acknowledgments: We also thank the National Institute of Standards and Technology for the use of their transmission electron microscope facilities during part of this work.

References

[1]K. Wakino, K. Minai, and H. Tamura, ''Microwave Characteristics of $(Zr,Sn)TiO_4$ and BaO–PbO–Nd_2O_3–TiO_2 Dielectric Resonators,'' *J. Am. Ceram. Soc.,* **67** [4] 278–81 (1984).

[2]T. Negas, G. Yeager, S. Bell, and R. Amren, ''Chemistry and Properties of Temperature Compensated Microwave Dielectrics''; pp. 21–38 in NIST Special Publication No. 804, *Chemistry of Electronic Ceramic Materials.* Edited by P. K. Davies and R. S. Roth. National Institute of Standards and Technology, Washington, DC, 1990.

[3]S. Kawashima, M. Nishida, I. Ueda, and H. Ouchi, ''$Ba(Zn_{1/3}Ta_{2/3})O_3$ Ceramics with Low Dielectric Loss at Microwave Frequencies, '' *J. Am. Ceram. Soc.,* **66** [6] 421–23 (1983).

[4]K. Matsumoto, T. Hiuga, K. Takada, and H. Ichimura, ''$Ba(Mg_{1/3}Ta_{2/3})O_3$ Ceramics with Ultra-Low Loss at Microwave Frequencies''; pp. 118–21 in Proceedings of the 6th IEEE International Symposium on Application of Ferroelectrics (June 1986). Institute of Electrical and Electronic Engineers, New York, 1986.

[5]R. Christoffersen and P. K. Davies, ''Structure of Commensurate and Incommensurate Ordered Phases in the System $ZrTiO_4$–$Zr_5Ti_7O_{24}$,'' *J. Am. Ceram. Soc.,* **75** [3] 563–69 (1992).

[6]R. Christoffersen, P. K. Davies, X. Wei, and T. Negas, ''Microstructure and Properties of Sn-Doped $ZrTiO_4$ Microwave Ceramics,'' *J. Am. Ceram. Soc.,* **77** [6] 1441–51 (1994).

[7]P. K. Davies and R. Christoffersen, ''Influence of Structural Defects on the Properties of Zirconium Titanate-Based Microwave Ceramics,'' *Proc. Br. Ceram. Soc.,* **52,** 13–27 (1994).

[8]P. K. Davies and R. S. Roth, ''Defect Intergrowths in Barium Polytitanates, 1. $Ba_2Ti_9O_{20}$,'' *J. Solid State Chem.,* **71,** 490–502 (1987).

[9]P. K. Davies and R. S. Roth, ''Defect Intergrowths in Barium Polytitanates, 2. $BaTi_5O_{11}$,'' *J. Solid State Chem.,* **71,** 503–12 (1987).

[10]P. K. Davies, ''Influence of Structural Defects on the Dielectric Properties of Ceramic Microwave Resonators''; pp. 137–52 in Ceramic Transactions, Vol. 53, *Materials and Processes for Wireless Communications.* Edited by T. Negas and H. Ling. American Ceramic Society, Westerville, OH, 1995.

[11]T. Negas and P. K. Davies, ''Influence of Chemistry and Processing on the Electrical Properties of $Ba_{6-3x}Ln_{8+2x}Ti_{18}O_{54}$ Solid Solutions''; pp. 179–96 in Ceramic Transactions, Vol. 53, *Materials and Processes for Wireless Communications.* Edited by T. Negas and H. Ling. American Ceramic Society, Westerville, OH, 1995.

[12]F. Galasso and J. Pyle, ''Ordering in Compounds of the $A(B'_{0.33}Ta_{0.67})O_3$ Type,'' *Inorg. Chem.,* **2** [3] 482–84 (1963).

[13]F. Galasso and J. Pyle, ''Preparation and Study of Ordering in $A(B'_{0.33}Nb_{0.67})O_3$ Perovskite-Type Compounds,'' *J. Phys. Chem.,* **67,** 1561–62 (1963).

[14]A. J. Jacobson, B. M. Collins, and B. E. F. Fender, ''A Powder Neutron and X-ray Diffraction Determination of the Structure of $Ba_3Ta_2ZnO_9$: An Investigation of Perovskite Phases in the System Ba–Ta–Zn–O and the Preparation of $Ba_2TaCdO_{5.5}$ and $Ba_2CeInO_{5.5}$,'' *Acta Crystallogr.,* **B32,** 1083–87 (1976).

[15]S. B. Desu and H. M. O'Bryan, ''Microwave Loss Quality of $BaZn_{0.33}Ta_{0.67}O_3$ Ceramics,'' *J. Am. Ceram. Soc.,* **68** [10] 546–51 (1985).

[16]I.-T. Kim, T.-S. Oh, and Y.-H. Kim, ''Lattice Distortion of $Ba(Zn_{1/3}Ta_{2/3})O_3$ with Ordering of B-site Cations,'' *J. Mater. Sci. Lett.,* **12,** 182–84 (1993).

[17]H. Tamura, T. Konoike, Y. Sakabe, and K. Wakino, ''Improved High Q Dielectric Resonator with Complex Perovskite Structure,'' *J. Am. Ceram. Soc.,* **67** [4] C-59–C-61 (1984).

[18]P. Woodward, R.-D. Hoffmann, and A. W. Sleight, ''Order–Disorder in $A_2M^{3+}M^{5+}O_6$ Perovskites,'' *J. Mater. Res.,* **9** [8] 2118–27 (1994).

[19]B. W. Hakki and P. D. Coleman, ''A Dielectric Method of Measuring Inductive Capacities in the Millimeter Range,'' *IEEE Trans. Microwave Theory Tech.,* **MTT-8,** 402–10 (1980).

[20]W. E. Courtney, ''Analysis and Evaluation of a Method of Measuring the Complex Permittivity and Permeability of Microwave Insulators,'' *IEEE Trans. Microwave Theory Tech.,* **MTT-18,** 476–85 (1970).

[21]D. Kajfez and P. Guillion, *Dielectric Resonators;* pp. 327–76. Artech House, Norwood, MA, 1986.

[22]F. S. Galasso, *Perovskite and High T_c Superconductors;* pp. 3–72. Gordon and Breach, New York, 1990.

[23]C. A. Randall and A. S. Bhalla, ''Nanostructural–Property Relations in Complex Lead Perovskites,'' *Jpn. J. Appl. Phys.,* **29,** 327–33 (1990).

[24]M. P. Harmer, J. Chen, P. Peng, H. M. Chan, and D. M. Smyth, ''Control of Microchemical Ordering in Relaxor Ferroelectrics and Related Compounds,'' *Ferroelectrics,* **97,** 263–74 (1989).

[25]J. Chen, H. Chan, and M. P. Harmer, ''Ordering Structure and Dielectric Properties of Undoped and La/Na-doped $Pb(Mg_{1/3}Nb_{2/3})O_3$,'' *J. Am. Ceram. Soc.,* **72** [4] 593–98 (1989).

[26]E. L. Colla, I. M. Reaney, and N. Setter, ''Effect of Structural Changes in Complex Perovskites on the Temperature Coefficient of the Relative Permittivity,'' *J. Appl. Phys.,* **74** [5] 3414–25 (1993).

[27]D. Viehland, Z. Xu, and D. Payne, ''Origin of F-spots and Stress-Sensitivity in Lanthanum Lead Zirconate Titanate,'' *J. Appl. Phys.,* **74,** 7454–58 (1993).

[28]H. Matsumoto, H. Tamura, and K. Wakino, ''$Ba(Mg,Ta)O_3$–$BaSnO_3$ High-Q Dielectric Resonator,'' *Jpn. J. Appl. Phys.,* **30,** 2347–49 (1991).

[29]E. J. Fresia, L. Katz, and R. Ward, ''Cation Substitution in Perovskite-like Phases,'' *J. Am. Chem. Soc.,* **81,** 4783–85 (1959).

[30]A. W. Sleight, J. M. Longo, and R. Ward, ''Compounds of Osmium and Rhenium with the Ordered Perovskite Structure,'' *Inorg. Chem.,* **1,** 245–50 (1959).

[31]G. Blasse, ''New Compounds with Perovskite-like Structures,'' *J. Inorg. Nucl. Chem.,* **27,** 993–1003 (1965).

[32]L. Padel, P. Poix, and A. Michel, ''Preparation and Crystallographic Studies of the System $Ba_2(UMg)O_6$–$Ba_2(U_{2/3}Fe_{4/3})O_6$,'' *Rev. Chim. Mineral.,* **9,** 337–50 (1972).

[33]A. D. Hilton, D. J. Barber, D. A. Randall, and T. R. Shrout, ''On Short Range Ordering in the Perovskite Lead Magnesium Niobate,'' *J. Mater. Sci.,* **25,** 3461–66 (1990).

[34]K. Park, L. Salamanca-Riba, M. Wuttig, and D. Viehland, ''Ordering in Lead Magnesium Niobate Solid Solutions,'' *J. Mater. Sci.,* **29,** 1284–89 (1994).

[35]D. Viehland, N. Kim, Z. Xu, and D. A. Payne, ''Structural Studies of Ordering in the $(Pb_{1-x}Ba_x)(Mg_{1/3}Nb_{2/3})O_3$ Crystalline Solution Series,'' *J. Am. Ceram. Soc.,* **78** [9] 2481–89 (1995).

[36]L.-J. Jin and T. B. Wu, ''Ordering Behavior of Lead Magnesium Niobate Ceramics with A-site Substitution,'' *J. Am. Ceram. Soc.,* **73** [5] 1253–56 (1990).